Physica B 404 (2009) 1509–1514

Contents lists available at ScienceDirect

Physica B

journal homepage: www.elsevier.com/locate/physb

Synthesis and characterization of single-phase Mn-doped ZnO

S. Chattopadhyay [a], S. Dutta [a], A. Banerjee [a], D. Jana [a], S. Bandyopadhyay [a,*], S. Chattopadhyay [b], A. Sarkar [c]

[a] Department of Physics, University of Calcutta, 92 Acharya Prafulla Chandra Road, Kolkata 700 009, West Bengal, India
[b] Department of Physics, Taki Government College, Taki 743 429, West Bengal, India
[c] Department of Physics, Bangabasi Morning College, 19 Rajkumar Chakraborty Sarani, Kolkata 700 009, West Bengal, India

ARTICLE INFO

Article history:
Received 23 July 2008
Received in revised form
31 December 2008
Accepted 8 January 2009

PACS:
73.40.Lq
61.72.−y
61.05.C

Keywords:
Semiconductor
Defects
X-ray diffraction

ABSTRACT

Different samples of $Zn_{1-x}Mn_xO$ series have been prepared using conventional solid-state sintering method. We identified up to what extent doping will enable us to synthesize single-phase polycrystalline Mn-doped ZnO sample, which is one of the prerequisites for dilute magnetic semiconductor, and we have analyzed its some other physical aspects. In synthesizing the samples, proportion of Mn varies from 1 to 5 at%. However, the milling time varied (6, 12, 24, 48 and 96 h) only for 2 at% Mn-doped samples while for other samples (1, 3, 4 and 5 at% Mn doped) the milling time has been fixed to 96 h. Room-temperature X-ray diffraction (XRD) data reveal that all of the prepared samples up to 3 at% of Mn doping exhibit wurtzite-type structure, and no segregation of Mn and/or its oxides has been found. The 4 at% Mn-doped samples show a weak peak of $ZnMn_2O_4$ apart from the other usual peaks of ZnO and the intensity of this impurity peak has been further increased for 5 at% of Mn doping. So beyond 3 at% doping, single-phase behavior is destroyed. Band gap for all the 2 at% Mn-doped samples has been estimated to be between 3.21 and 3.19 eV and the reason for this low band gap values has been explained through the grain boundary trapping model. The room-temperature resistivity measurement shows an increase of resistivity up to 48 h of milling and with further milling it saturates. The defect state of these samples has been investigated using the positron annihilation lifetime (PAL) spectroscopy technique. Here all the relevant lifetime parameters of positron i.e. free annihilation (τ_1) at defect site (τ_2) and average (τ_{av}) increases with milling time.

1. Introduction

The wide applications of spintronic devices such as spin-valve transistor, spin-light emitting diodes, non-volatile memory, optical isolator, ultrafast optical switches, inspires extensive research work to synthesize diluted magnetic semiconductors (DMSs) with III–V and II–VI semiconductors [1–16]. Quite a substantial amount of work has been done with transition metal (Tm)-doped III–V semiconductors particularly Mn-doped GaAs [2,3]. The highest reported ferromagnetic Curie temperature (T_C) in this system is ~172 K, which is much lower than room temperature. Dietl et al. [17] predicted high-temperature ferromagnetism in magnetically doped wide band gap p-type semiconductors particularly in ZnO, GaN, GaAs and ZnTe. This fact has motivated researchers to study the properties of Tm-doped semiconductors. Room-temperature ferromagnetism has been reported by Sharma et al. [1] and Milivojevic et al. [10] in polycrystalline $Zn_{1-x}Mn_xO$ samples, prepared using solid-state sintering route. ZnO-based DMS system has some advantages over the other because of some of its unique characteristics like large band gap (~3.4 eV), large exciton binding energy at room temperature (~60 meV), high optical gain (300 cm^{-1}) and very short luminescence lifetime [11], which are required for various optoelectronic [12] and magneto-optical [13] devices.

In this work, we have made a systematic study of structural, optical, electrical properties and defect analysis through positron annihilation lifetime (PAL) spectroscopy of 5 different 2 at% Mn-doped samples prepared by solid-state sintering method at different milling times. Study of structural properties has also been performed for 1, 2, 3, 4 and 5 at% Mn-doped samples prepared with 96 h of milling. Structural characterization was made through X-ray diffractometry (XRD). A primary requisition for DMS material is that the structure of the material must be of single phase. This is required because the chances of ferromagnetic ordering due to segregation of magnetic ions arising out of doping of transition metals into an impurity phase or any other precipitate would be zero. Though it is true that some of the impurity phase(s) in ZnMnO bear ferromagnetism, ferromagnetism originating from the impurity phases cannot have the desired properties for spintronic devices such as spin injection [18]. So the extent of doping by Tm has definitely a limit beyond which multi-phase components start to arise. In this work we have estimated

* Corresponding author. Fax: +91 33 2351 9755.
E-mail address: sbaphy@caluniv.ac.in (S. Bandyopadhyay).

0921-4526/$ - see front matter © 2009 Elsevier B.V. All rights reserved.
doi:10.1016/j.physb.2009.01.008

the maximum amount of dopant (Mn) incorporation in the host material ZnO for samples derived out of solid-state sintering method and hence no signature of impurity phase has been developed.

Room-temperature resistivities were also recorded and optical studies were done by UV–visible (UV–vis) absorption spectroscopy. It is an established fact that ferromagnetism in DMS materials is carrier mediated [19]. In Mn-doped ZnO the study on defect states will be crucial as defects are proposed to generate free carriers [20] in ZnO. Such defects may play a significant role in achieving ferromagnetism [21]. In his pioneering work, Dietl et al. [17] pointed out that the defect state plays an important role for showing ferromagnetism in these types of materials. Iusan et al. [22] and Hasu et al. [23] have conducted interesting theoretical work on establishing the role of defects on ferromagnetism in Tm-doped ZnO. But there is hardly any experimental study to analyze the role of defect state not only in Tm-doped ZnO samples but also in any other DMS material. We have made a systematic study of the $Zn_{0.98}Mn_{0.02}O$ samples using room-temperature PAL. Positron lifetimes inside a material (~100–400 ps) can be measured from PAL spectroscopy. Positrons from a radioactive source (here ^{22}Na) are injected into the material and they get thermalized within 1–10 ps. Then they annihilate an electron of that material. It is well known that positrons are preferentially populated in low electron concentration regions. Positrons can be trapped in defects present in the material. The lifetime of trapped positrons in defects is comparatively longer with respect to those which annihilate at defect-free regions. Hence, the analysis of PAL spectrum may provide some interesting results regarding the nature and abundance of defects.

2. Experimental details

Five different 2 at% Mn-doped ZnO ($Zn_{1-x}Mn_xO$) have been prepared through conventional solid-state sintering method [1] using ZnO (99.99%, Sigma-Aldrich, Germany) and MnO_2 (99.9%, Sigma-Aldrich, Germany) at different milling times (6, 12, 24, 48 and 96 h). The stoichiometric amounts of samples have been taken. The samples were milled first for different durations using "Fritsch planetary mono mill" (Model no: pulverisette 6). The milling has been performed in two stages. The first milling time was one-third of the total milling time for a particular sample. Next they were sintered first at 400 °C for 8 h and finally, after making pallets, they were sintered at 500 °C for 12 h using digital furnace. In between the two sintering processes, the samples were milled with remaining two-third of the total milling time. The ball to mass ratio was maintained at 1:1 throughout the milling process. The final annealing temperature was 500 °C as it was reported that the samples annealed at 500 °C shows room-temperature ferromagnetism [1,18,24] and decreases with annealing above 500 °C [1,24]. Garcia et al. further showed that in presence of Zn, the transformation of Mn^{+4} states to Mn^{+3} states starts at about 200 °C. The transformation is completed at about 600 °C. Now ferromagnetism in MnZnO system arises when Mn^{+3} and Mn^{+4} states coexist. Therefore we expect a substantial portion of Mn^{+4} states transformed into Mn^{+3} states at the annealing temperature around 500 °C. This is the reason for choosing 500 °C as final annealing temperature. We have also prepared five different samples of $Zn_{1-x}Mn_xO$ series by varying the proportion of Mn from 1 to 5 at% with 96 h of milling keeping all other conditions unaltered.

The XRD data have been collected in a Philips PW 1830 automatic powder diffractometer with CuK_α radiation. The range of scanning is 10–80° (2θ) in a step size of 0.01°. We have calculated the crystallite size using Scherrer's formula [25]. The contribution of instrumental broadening has been taken into account.

The variation of band gap with milling time has been investigated by UV–vis absorption spectroscopy using Hitachi U-3501 spectrophotometer in the wavelength range 200–1600 nm at room temperature.

Room-temperature resistivity measurement has been carried out in usual two-probe technique using Keithley 6514 Electrometer, because of high resistive samples.

For positron annihilation study, a 10-μCi ^{22}Na positron source (enclosed in thin mylar foil) has been sandwiched between two identical plane faced pallets of the samples. We have measured the PAL spectra with a fast–slow coincidence assembly [26] having 182 ± 1 ps time resolution. Measured spectra have been analyzed by the computer program PATFIT-88 [27] with necessary source correction to obtain the possible lifetime components τ_i and their corresponding intensities I_i.

3. Result and discussion

XRD patterns of all $Zn_{0.98}Mn_{0.02}O$ (prepared at different milling times, 6, 12, 24, 48 and 96 h) are shown in Fig. 1. The indices in the spectra of Fig. 1 indicate the expected positions of the peaks for the wurtzite-crystal structure of ZnO, no signature of impurity peaks has been observed [10]. This indicates that Mn might have been substitutionally incorporated in ZnO lattice and so no impurity phase has been formed. The above observation is also

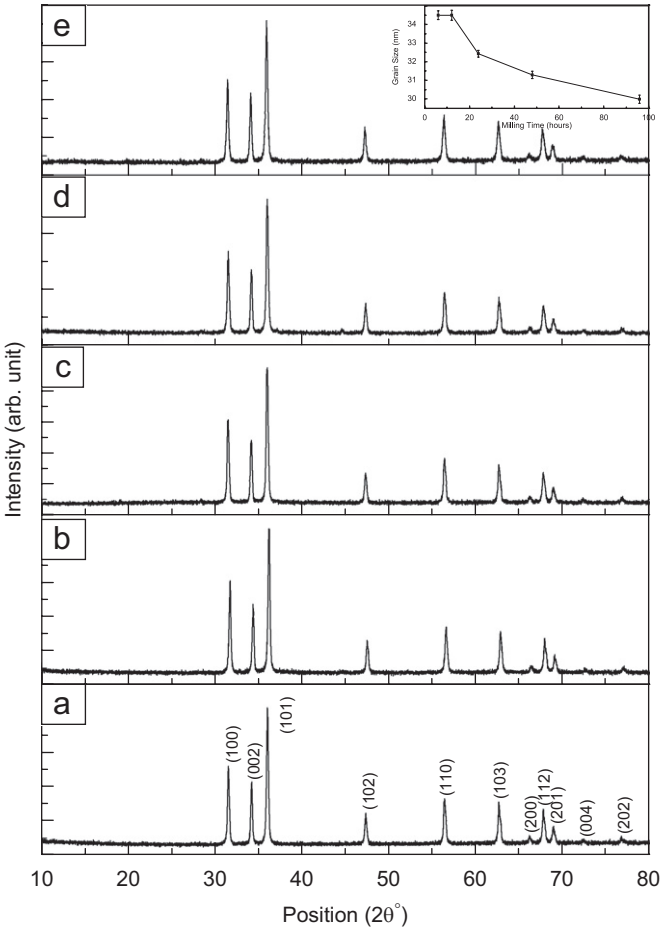

Fig. 1. XRD spectra of (a) 6, (b) 12, (c) 24, (d) 48 and (e) 96 h milled 2 at% Mn-doped ZnO samples. Inset: variation of grain size with milling time of 2 at% Mn-doped ZnO samples prepared at different milling times as calculated using Sherrerr formula and (101) peak.

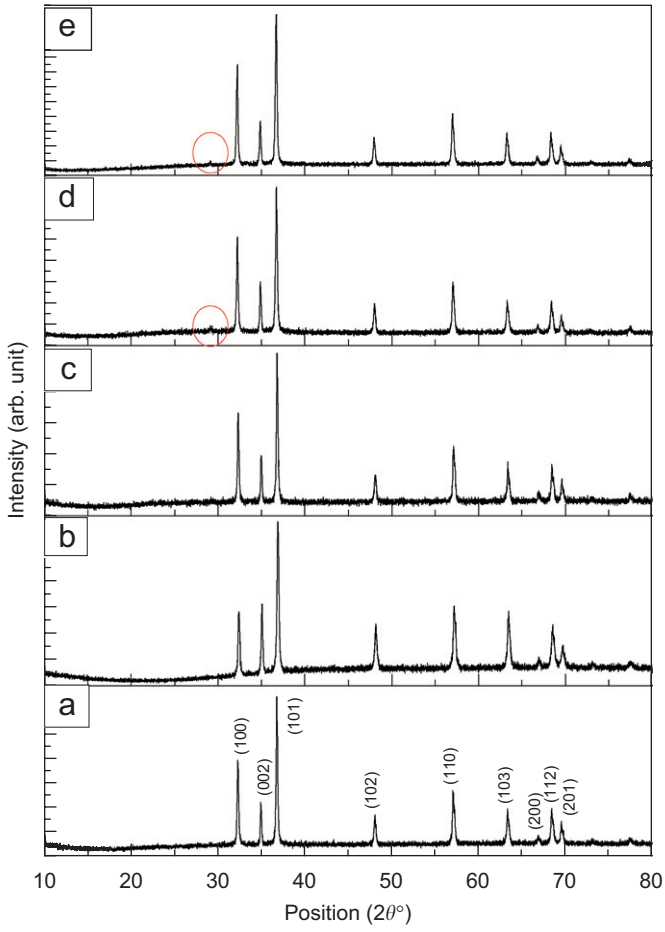

Fig. 2. XRD spectra of 96 h milled (a) 1 at%, (b) 2 at%, (c) 3 at%, (d) 4 at% and (e) 5 at% Mn-doped ZnO samples.

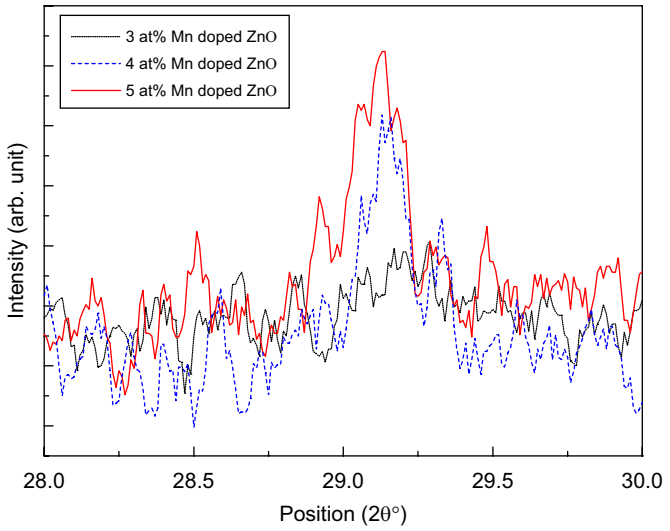

Fig. 3. Exaggerated plotting of XRD spectra in the range 2θ from 28° to 30° for 3, 4 and 5 at% Mn-doped ZnO samples.

Table 1
Value of grain size, band gap and room temperature resistivity of $Zn_{0.98}Mn_{02}O$ samples prepared at different milling times.

Milling time (h)	Grain size (nm)	Band gap (eV)	Room-temperature resistivity (MΩ cm)
6	34.50±0.24	3.21	4.64±0.12
12	34.49±0.27	3.21	72.09±0.57
24	32.44±0.18	3.20	219.44±5.59
48	31.29±0.20	3.19	250.58±6.39
96	29.99±0.22	3.19	239.19±5.65

true for the samples doped with 1 and 3 at% Mn prepared at 96 h of milling. When the proportion of Mn has been increased to 4 at%, a weak (1 1 2) peak of $ZnMn_2O_4$ has been observed at 29.11° (2θ), with further increase of proportion of Mn to 5 at% the intensity of this (1 1 2) peak of $ZnMn_2O_4$ slightly increased, as shown in Fig. 2. The growing tendency of intensity of the impurity peak in cases of 5 at% doped sample has been shown clearly in Fig. 3 with exaggerated plotting only in the range of 2θ from 28° to 30° for 3, 4 and 5 at% Mn-doped samples. From Fig. 2 it may appear that the growing up of (1 1 2) peak of $ZnMn_2O_4$ around 29° starts from 3 at% Mn-doped samples but careful observation of Fig. 3 strongly shows that the (1 1 2) peak of $ZnMn_2O_4$ starts growing from 4 at% doping. Actually the formation of impurity phase in case of lightly doped semiconductors depends on the inability of the power of the dopants (here transition metal Mn) to replace substitutionally the cation (here Zn) of the host compound semiconductor. Now, up to 3 at% level of doping Mn can substitutionally replace Zn but when the degree of doping exceeds further to 4 at% and above, not all of the Mn atoms replace Zn atoms rather segregated as $ZnMn_2O_4$. As single-phase formation is one of the primary criterions in our samples, doping concentration cannot be increased beyond 3 at% in this solid-state sintering method for Mn-doped ZnO samples. The effect of crystallite-size-induced broadening has been analyzed using Sherrerr's formula using the (1 0 1) peak, as shown in the inset of Fig. 1. The crystalline size can be obtained using the following relation:

$$D = \frac{K\lambda}{\beta \cos\theta}$$

where β is FWHM in radians, D the average crystallite size, K the shape factor (usually taken 0.89), λ the X-ray wavelength and θ the Bragg angle. The estimated grain size of the 2 at% Mn-doped samples has been found to be varying from 34.5 to 30 nm and plotted in the inset of Fig. 1. The values of grain size for different 2 at% Mn-doped samples prepared at different milling time are shown in Table 1. The little variation of grain size data indicates that milling time has no direct correlation with grain size.

UV–vis absorption spectra of all the 2 at% Mn-doped samples are shown in the inset of Fig. 4. According to Tauc et al. [28] and Pancov [29] for a given transition, photon energy $h\upsilon$ can be related to band gap energy (E_g) by the following expression:

$$\alpha = \frac{A(h\upsilon - E_g)^{m/2}}{h\upsilon}$$

where $m = 1$ for a direct transition and $m = 4$ for an indirect transition, α is the absorption coefficient and A is a constant. As ZnO is a direct band gap semiconductor, we have calculated the band gap of these samples from linear fitting to the $(\alpha h\upsilon)^2$ against energy (E) plot as shown in Fig. 4 and the value of band gap obtained for all the samples is in between 3.21 and 3.19 eV, which is slightly less than for generally reported [30] value 3.4 eV. In one of the earlier works [31] of our group, it was calculated as 3.22 eV for pure ZnO powders. Nevertheless, the reduction in band gap might be due to a smaller average grain size and possibly lower carrier concentration (because of the high value of resistivity to be shown below) in our samples. To explain this small variation of the band gap of our Mn-doped ZnO samples, we introduce a variant of a simple model proposed earlier for ZnO film on fused silica [32] and glass substrate [33]. As a result of this intuitive

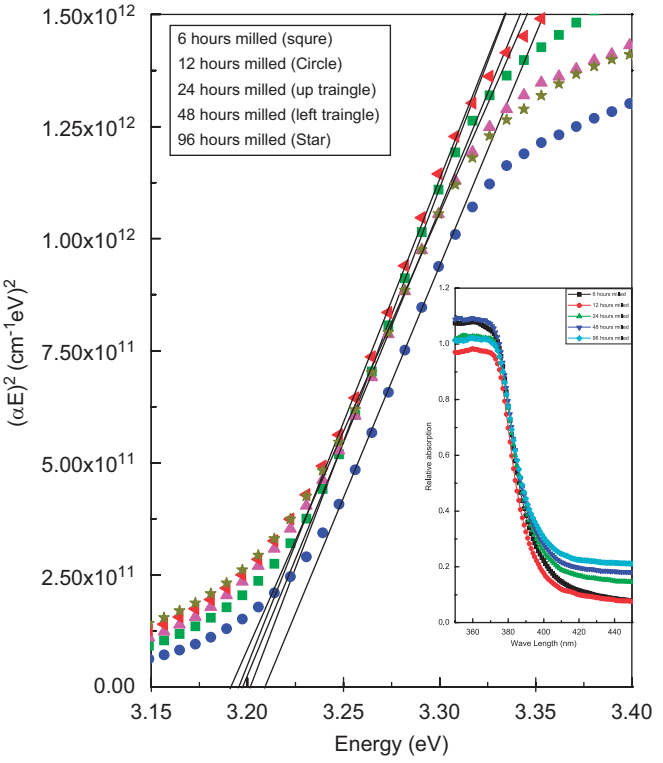

Fig. 4. Energy vs. $(\alpha E)^2$ plot of the 2 at% Mn-doped ZnO samples prepared by varying milling time. Insets UV–vis spectra of the 2 at% Mn-doped ZnO samples prepared by varying milling times.

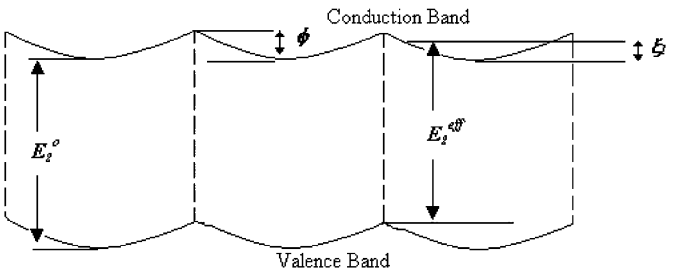

Fig. 5. Idealized 1D potential variation for several grains which are assumed to be of the same size and to have the same trap density.

picture, periodic variations in potential within the grain do occur due to trapping of impurities arising out of Mn doping. This manifests naturally in a non-uniform variation of the electric fields at the grain boundaries. This causes a vertical band gap, which is the difference between the highest point of valence band and the lowest point of conduction band. An idealized periodic potential diagram with important parameters marked on it is shown schematically in Fig. 5. From the diagram it can be seen that the effective band gap E_g^{eff} is given by

$$E_g^{eff} = E_g^0 - \phi + \xi_1$$

where E_g^0 is the original gap, ϕ the barrier height at the grain boundary and ξ_1 the first quantized level of a 1D gas. Using Scherrer's formula, we find the variation of average grain size lies between 30 and 34 nm. This indicates a band bending of 0.2016 eV. This is consistent with the observed difference of the band gap of the samples. This justifies that the model chosen for analyzing the optical data seems to be a proper one.

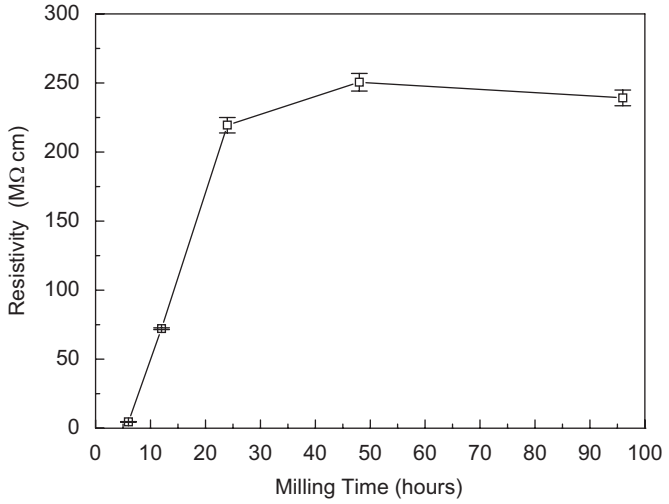

Fig. 6. Variation of room-temperature resistivity with milling time for different 2 at% Mn-doped ZnO samples.

In Fig. 6, the variation of room-temperature resistivity with milling time has been shown. The room-temperature resistivity increases with milling time up to 48 h and later there is an indication of attaining saturation in resistivity value, as is also evident from Table 1. Moreover, the value of the resistivity is less for the 6 and 12 h milled samples compared to that of pure ZnO ($8.4 \times 10^7\,\Omega$ cm) [33]. But for samples milled with longer periods such as 24, 48 and 96 h, the resistivity becomes very high. The possible reason behind this might be that the inherent non-stoichiometry present in the ZnO matrix is dissolved with longer period of milling. The oxygen vacancy present in the system of ZnO is responsible for a comparatively low value of resistivity in case of the sample with milling times 6 and 12 h. There are two competitive effects: sintering at 500 °C increases the density of oxygen vacancy and milling tries to make the sample stoichiometric by decreasing the density of oxygen vacancy. When the milling time is only 6 or 12 h, the former one predominates over the later one, so the resistivity decreases and reaches below the value of pure ZnO. The resistivity of pure ZnO was observed without sintering and milling also. But when the period of milling gradually increases from 12 to 48 h and as the period and temperature of sintering remain the same, the latter effect dominates over the former one giving rise to a significant increase in resistivity. With further increase in milling time, the specimen becomes less oxygen deficient, its resistivity increases and nearly saturates after 48 h of milling.

To elucidate the above intuitive picture, we have performed PAL analysis and the results are shown in Fig. 7 and Table 2. All lifetime spectra are best fitted with three-components lifetime fit. The longest ($\geqslant$1248 ps with intensity 3–4%) among them is the third one (τ_3). Positron annihilation from orthopositronium like atoms contributes for τ_3. Orthopositronium formation inside the microvoids [24] is always present within the materials. It decays into parapositronium through pickoff annihilation, giving rise to such a large lifetime. In polycrystalline samples, voids (that favors positronium formation) are always present [31,34]. But positronium is normally found in a defect free solid in a self-trapped state, i.e. positronium creates by itself a "cage" by pushing away the surrounding atoms [35]. Hence the origin of τ_3 within materials is different and not related to the positron trapping at defects. The shortest lifetime component τ_1 comes up due to the free annihilation of positrons [24,34,36]. The effects of small vacancies (like mono-vacancies, etc.) [37–40] or shallow vacancies (like oxygen vacancies [39] in ZnO) may also be related with τ_1 in

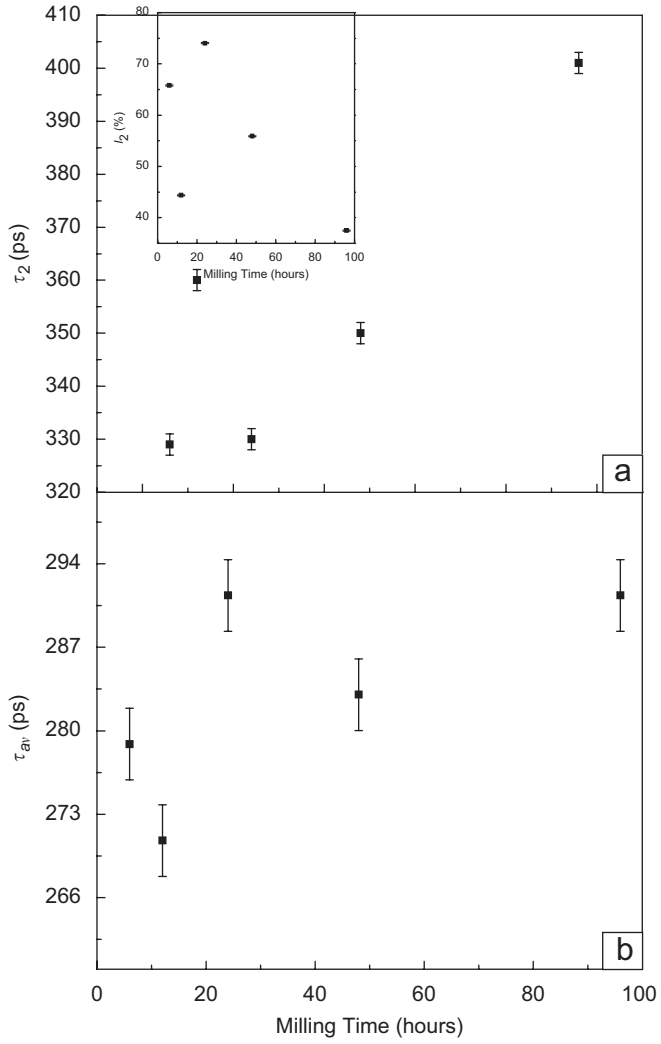

Fig. 7. Variation of (a) positron lifetime annihilating at defect site (τ_2) and (b) average positron lifetime (τ_{av}) with milling time for 2 at% Mn-doped ZnO samples. The inset shows variation of I_2 (intensity corresponding to τ_2) with milling time.

Table 2
Fitting parameters found from positron annihilation lifetime measurement on $Zn_{0.98}Mn_{02}O$ samples prepared at different milling times.

Milling time (h)	τ_1 (ps)	I_1 (%)	τ_3 (ps)	I_3 (%)
6	171 ± 1	30.56 ± 0.1	1349 ± 31	3.6 ± 0.2
12	195 ± 1	52.21 ± 0.1	1439 ± 32	3.4 ± 0.2
24	163 ± 1	22.30 ± 0.1	1317 ± 32	3.7 ± 0.2
48	190 ± 1	40.23 ± 0.1	1248 ± 31	3.9 ± 0.2
96	222 ± 1	59.30 ± 0.1	1406 ± 48	3.2 ± 0.2

case of disordered systems. Though τ_1 itself is a weighted average of free and trapped annihilation these sites are not major positron traps. We have found (shown in Table 2) that there is an increase in the value of τ_1 with milling time. The above-mentioned two competitive effects, sintering and milling, may also be responsible for this kind of variation of τ_1. Oxygen vacancy has been increased by sintering at 500 °C which inturn increases the electron density within the sample whereas milling tries to make the sample stoichiometric by decreasing the density of oxygen vacancy, which implies a decrease in free electron density. We have gradually increased the period of milling from 6 to 96 h with the period and temperature of sintering remaining same. With the increase of the milling time, the effect of milling predominates over the sintering effect so the available electron density reduced and it is manifested both in resistivity data and τ_1. Here a point is worth noting: Reduction in carrier density may originate in localization of electrons into some open volume defects which inturn increases both resistivity and τ_1.

The most important component of positron lifetime is τ_2 which indicates qualitatively the nature and size of the vacancy [39] and its relative intensity gives a quantitative measure of abundance of that vacancy with respect to some standard of the same sample. We have found considerable increase in the τ_2 values with increasing milling time from 6 to 96 h (Fig. 7(a)). Variation of corresponding intensities (I_2) is given in the inset of Fig. 7(a). From τ_1, I_1, τ_2 and I_2 the average positron lifetime $\tau_{av} = [\tau_1 I_1 + \tau_2 I_2 / I_1 + I_2]$ can be calculated. τ_{av} shows an overall increase with milling time similar to that of τ_2. This might occur because of the increase in defect clustering near the grin boundary due to mechanical milling. The thermal energy given to the system by the sintering process may help the intra-grain Zn vacancies to approach the grain surfaces, which are the universal sink of defects. In this way, small-size Zn vacancies (mono-vacancies, etc.) assemble near the grain surfaces and give rise to τ_1 (shown in Table 2). A fraction of such mono-vacancies joins together to form larger size vacancy clusters causing an increase in the value of τ_2 also.

4. Conclusion

In this present work we have characterized the $Zn_{1-x}Mn_xO$ using room-temperature XRD, UV–vis absorption spectroscopy, room-temperature resistivity and room-temperature PAL spectroscopy. From the results of these characterizations, the following conclusions can be drawn.

Room-temperature XRD results indicate that all the samples, except 4 and 5 at% Mn-doped sample exhibit wurtzite-type structure, similar to that of stoichiometric ZnO. No segregation of Mn and/or its oxides has been found. This signifies that Mn might have been substitutionally incorporated in the ZnO lattice for these samples. The 4 and 5 at% Mn-doped samples show a weak peak of $ZnMn_2O_4$ apart from the usual other peaks of ZnO. The intensity of this peak increases with increasing Mn concentration. It is highly indicative of the extent of doping of magnetic species, which will be useful to achieve intrinsic ferromagnetic ordering.

Band gap for all the Mn-doped samples has been estimated to be between 3.21 and 3.19 eV. This indicate that slight decrease in band gap values in Mn-doped ZnO samples in comparison to that of the un-doped ZnO sample is due to band bending. The reason for this bending is shown to be the periodic variation of grain boundary potential. The amount of band bending estimated from grain size (calculated from XRD data) is consistent with the values of the band gap calculated from optical measurements.

The room-temperature resistivity increases from 4.64 to 239.14 MΩ cm with milling time varying from 6 to 48 h and for the sample milled for 96 h, there is an indication of saturation in the resistivity values. The reason behind this might be that with longer period of milling (from 6 to 96 h) the reduction of proportion of the oxygen vacancies, which are one of the sources of free electrons in the ZnO matrix, is reduced.

PAL analysis shows that there is an increase in the value of τ_1 with milling time. This is due to decrease in available electron density. Electrons may localize into some open volume defects, which inturn increase both resistivity and τ_1. Considerable increase in τ_2 and τ_{av} values with milling time has been found and it is due to increase in defect clustering near the grain boundary due to mechanical milling.

Acknowledgements

We are grateful to DST-FIST for providing financial assistance. Two of the authors (S.C.[a] and S.D.) are grateful to Government of West Bengal for providing financial assistance in the form of University Research Fellowship. One of the authors (S.B.) is also thankful to DST for providing grant in a research project with sanction no. SF/FTP/PS-31/2006 dated 20.09.2007. We also like to acknowledge Mr. Manas Sutradhar, Department of Chemistry, University of Calcutta, for helping us in performing UV–vis spectroscopy experiment.

References

[1] P. Sharma, A. Gupta, K.V. Rao, F.J. Owens, R. Sharma, R. Ahuja, J.M.O. Guillen, B. Johansson, G.A. Gehring, Nat. Mater. 2 (2003) 673.
[2] A.M. Nazmul, S. Kobayashi, S. Sugahara, M. Tanaka, Physica E 21 (2004) 937.
[3] T. Jungwirth, K.Y. Wang, J. Mašek, K.W. Edmonds, J. König, J. Sinova, M. Polini, N.A. Goncharuk, A.H. MacDonald, M. Sawicki, A.W. Rushforth, R.P. Campion, L.X. Zhao, C.T. Foxon, B.L. Gallagher, Phys. Rev. B 72 (2005) 165204.
[4] O.D. Jayakumar, I.K. Gopalakrishnan, S.K. Kulshrestha, Physica B 381 (2006) 194.
[5] K. Ueda, H. Tabata, T. Kawai, Appl. Phys. Lett. 79 (2001) 988.
[6] G.T. Thaler, M.E. Overberg, B. Gila, R. Frazier, C.R. Abernathy, S.J. Pearton, J.S. Lee, S.Y. Lee, Y.D. Park, Z.G. Khim, J. Kim, F. Ren, Appl. Phys. Lett. 80 (2002) 3964.
[7] K. Sato, H.K. Yoshida, Physica B 308–310 (2006) 904.
[8] S.A. Chambers, T. Droubay, C.M. Wang, A.S. Lea, R.F.C. Farrow, L. Folks, V. Deline, S. Anders, Appl. Phys. Lett. 82 (2003) 1257.
[9] J.H. Kim, H. Kim, D. Kim, Y. Eon, I. Woong, K. Choo, J. Appl. Phys. 92 (2002) 6066.
[10] D. Milivojevic, J. Blanusa, V. Spasojevic, V. Kusigerski, B. Babic-Stojic, Solid State Commun. 141 (2007) 641.
[11] R. Kumar, F. Singh, B. Angadi, J.W. Choi, W.K. Choi, K. Jeong, J.H. Song, M.W. Khan, J.P. Srivastava, A. Kumar, R.P. Tandon, J. Appl. Phys. 100 (2006) 113708.
[12] B.K. Meyer, H. Alves, D.M. Hofmann, W. Kriegseis, D. Forster, F. Bertram, J. Christen, A. Hoffmann, M. Straßburg, M. Dworzak, U. Haboeck, A.V. Rodina, Phys. Status Solidi B 241 (2004) 231.
[13] G. Lawes, A.S. Risbud, A.P. Ramirez, R. Seshadri, Phys. Rev. B 71 (2005) 045201.
[14] M. Ivill, S.J. Pearton, Y.W. Heo, J. Kelly, A.F. Hebard, D.P. Norton, J. Appl. Phys. 101 (2007) 123909.
[15] J. Zhang, R. Skomski, D.J. Sellmyer, J. Appl. Phys. 97 (2005) 10D303.
[16] A. Chartier, P. D'Arco, R. Dovesi, V.R. Saunders, Phys. Rev. B 60 (1999) 14042.
[17] T. Dietl, H. Ohno, F. Matsukura, J. Cibert, D. Ferrand, Science 287 (2000) 1019.
[18] J.L. Costa-Krämer, F. Briones, J.F. Fernández, A.C. Caballero, M. Villegas, M. Díaz, M.A. García, A. Hernando, Nanotechnology 16 (2005) 214.
[19] H.J. Lee, H.H. Nam, Y.C. Cho, S.K. Kim, C.H. Park, C.R. Cho, S.Y. Jeong, Eur. Phys. Lett. 78 (2007) 17001.
[20] A. Janotti, C.G. Van de Walle, Phys. Rev. B 76 (2007) 165202.
[21] A. Sundaresan, R. Bhargavi, N. Rangarajan, U. Suddesh, C.N.R. Rao, Phys. Rev. B 74 (2006) 161306.
[22] D. Iusan, B. Sanyal, O. Eriksson, Phys. Status Solidi A 204 (2007) 53.
[23] H.S. Hsu, J.C.A. Huang, S.F. Chen, C.P. Liu, Appl. Phys. Lett. 90 (2007) 102506.
[24] M.A. García, M.L. Ruiz-González, A. Quesada, J.L. Costa-Krämer, J.F. Fernández, S.J. Khatib, A. Wennberg, A.C. Caballero, M.S. Martín-González, M. Villegas, F. Briones, J.M. González-Calbet, A. Hernando, Phys. Rev. Lett. 94 (2005) 217206.
[25] B.E. Waren, X-ray Diffraction, Addison-Wesley, Reading, MA, 1969.
[26] S. Dutta, S. Chattopadhyay, A. Sarkar, M. Chakrabarti, D. Sanyal, D. Jana, Prog. Mater. Sci. 54 (2009) 89.
[27] P. Kirkegaard, N.J. Pedersen, M. Eldrup, Report of Riso National Lab, Riso-M-2740, 1989.
[28] J. Tauc, R. Grigorvici, Y. Yanca, Phys. Status Solidi 15 (1966) 627.
[29] J. Pancove, Optical Processes in Semiconductors, Prentice-Hall, Englewood Cliffs, NJ, 1979.
[30] D.C. Look, Mater. Sci. Eng. B 80 (2001) 383.
[31] S. Dutta, S. Chattopadhyay, D. Jana, A. Banerjee, S. Manik, S.K. Pradhan, M. Sutradhar, A. Sarkar, J. Appl. Phys. 100 (2006) 114328.
[32] V. Srikant, D.R. Clarke, J. Appl. Phys. 81 (1997) 6357.
[33] S. Bandyopadhyay, G.K. Paul, S.K. Sen, Sol. Energy Mater. Sol. Cells 71 (2002) 103.
[34] S. Dutta, M. Chakrabarti, S. Chattopadhyay, D. Jana, D. Sanyal, A. Sarkar, J. Appl. Phys. 98 (2005) 053513.
[35] R. Krause-Rehberg, H.S. Leipner, Positron Annihilation in Semiconductors, Springer, Berlin, 1999 Chapter 3, p. 61.
[36] Z.Z. Zhi, Y.C. Liu, B.S. Li, X.T. Zhang, Y.M. Lu, D.Z. Shen, X.W. Fan, J. Phys. D 36 (2003) 719.
[37] Z.Q. Chen, M. Meakawa, S. Yamamoto, A. Kawasuso, X.L. Yuan, T. Sekiguchi, R. Suzuki, T. Ohdaira, Phys. Rev. B 69 (2004) 035210.
[38] P.M.G. Nambissan, C. Upadhyay, H.C. Verma, J. Appl. Phys. 93 (2003) 6320.
[39] F. Tuomisto, K. Saarinen, D.C. Look, G.C. Farlow, Phys. Rev. B 72 (2005) 085206.
[40] P. Hautojarvi, C. Corbel, in: A. Dupasquier, A.P. Millis Jr., Positron Spectroscopy in Solids, IOS, Amsterdam, 1995, p. 491.